

Radiative Cooling in MHD Models of the Quiet Sun Convection Zone and Corona

W.P. Abbett¹ · G.H. Fisher¹

© Springer

Abstract We present a series of numerical simulations of the quiet Sun plasma threaded by magnetic fields that extend from the upper convection zone into the low corona. We discuss an efficient, simplified approximation to the physics of optically thick radiative transport through the surface layers, and investigate the effects of convective turbulence on the magnetic structure of the Sun's atmosphere in an initially unipolar (open field) region. We find that the net Poynting flux below the surface is on average directed toward the interior, while in the photosphere and chromosphere the net flow of electromagnetic energy is outward into the solar corona. Overturning convective motions between these layers driven by rapid radiative cooling appears to be the source of energy for the oppositely directed fluxes of electromagnetic energy.

Keywords: Convection; Corona; Magnetic fields; Photosphere; Radiative Transfer

1. Introduction

To understand the physics of solar activity, we must understand the magnetic and energetic connection between the Sun's convective envelope and corona. The magnetic fields that mediate or energize most, if not all, solar activity are generated below the visible surface within the turbulent convection zone. Yet most of what we can directly measure originates from the solar atmosphere, where physical conditions are fundamentally different from that of the interior. While helioseismic inversions provide an invaluable window into the physics of the Sun's interior, understanding the physical connection between subsurface features and those observed in the solar atmosphere requires a realistic forward model.

But what level of realism in a numerical model is necessary to describe the complex magnetic connectivity and energetics of the solar atmosphere lying between the visible surface and the corona? It is of great benefit, for example, to formulate a simple, well-defined problem, and set up an idealized numerical

¹ Space Sciences Laboratory, University of California, Berkeley, CA, USA
email: abbett@ssl.berkeley.edu, fisher@ssl.berkeley.edu

experiment that sheds light on the relevant physical processes in an otherwise complex system. In this way, important progress has been made in our understanding of the physics of magnetic flux emergence in highly stratified model atmospheres (see, *e.g.*, Manchester *et al.*, 2004; Murray *et al.*, 2006; Magara, 2006; Galsgaard *et al.*, 2007; Fan, 2009; Archontis and Hood, 2010).

Yet the observed evolution of the photospheric magnetic field is often far more complex, particularly in and around CME- and flare-producing active regions. It is difficult to set up a simple magnetic and energetic configuration and an associated physics-based photospheric boundary condition that can initialize a simulation of the solar atmosphere and faithfully mimic the coronal evolution of a complex active region. If we wish to perform first-principles quantitative studies of phenomena such as eruptive events, the energization of the solar wind, active region decay, the transport of magnetic free energy and helicity into the solar atmosphere, and the physics of coronal heating, it is essential to evolve a turbulent model convection zone and corona within a single, large-scale computational domain.

To achieve this, we must accommodate the fundamental energetics of the system while still retaining the ability to study the interplay between large and small-scale magnetic structures that evolve over different timescales. Clearly, radiative transport plays a critical role in the energy balance of the atmospheric layers that bridge the gap between the visible surface and corona. Surface cooling drives convection, and convective turbulence both generates magnetic field and mediates the flux of magnetic energy that enters the solar atmosphere. Yet the physics of radiative transport can be computationally expensive to treat realistically, even in the context of small-scale domains that do not include the convection zone and corona within a single computational volume. For example, energetically important transitions in the solar chromosphere are often decoupled from the local thermodynamic state of the plasma (a state of non-local thermodynamic equilibrium, or non-LTE) suggesting that a truly realistic numerical model must also couple the macroscopic radiative transfer and level population equations to the system of conservation equations (see, *e.g.*, McClymont and Canfield, 1983; Fisher, Canfield, and McClymont, 1985; Carlsson and Stein, 1992; Abbett and Hawley, 1999; Allred *et al.*, 2005). To complicate matters further, non-thermal physics, and the physics of ion-neutral drag may substantially affect the energy balance of the chromosphere (Krasnoselskikh *et al.*, 2010).

While it remains impractical to perform large-scale, 3D, non-LTE radiative MHD calculations without employing substantial approximations to make the system tractable, it is now common practice to realistically treat optically thick surface cooling in the upper convection zone and photosphere in LTE (a good approximation in these layers). There are many examples of thin-layer, high-resolution calculations that incorporate solutions to the non-gray radiative transfer equation in Cartesian domains that include the upper convection zone and extend into the low chromosphere (Bercik, 2002; Stein and Nordlund, 2006; Georgobiani *et al.*, 2007; Rempel, Schüssler, and Knölker, 2009; Cheung *et al.*, 2010). In addition, calculations that realistically treat radiative transfer have been applied to simulations of solar granulation in relatively small-scale domains that also include a transition region and corona (Martínez-Sykora, Hansteen, and Carlsson,

2008; Martínez-Sykora, Hansteen, and Carlsson, 2009; Carlsson, Hansteen, and Gudiksen, 2010).

Our goal, however, is to expand the size of such computational domains to active region or even global spatial scales while still retaining as realistic a thermodynamic environment as is feasible. Thus, we strive to develop the simplest model possible that allows us to capture the essential physics of the convection-zone-to-corona system while still maintaining the computational efficiency of models in which optically thick radiative cooling is treated in a parameterized fashion (*e.g.*, Abbett, 2007; Fang *et al.*, 2010a). In this way, we hope to make practical the performance of physics-based, first principles simulations, allowing for quantitative, parameter-space studies of processes such as filament formation, active region emergence and decay, and flare and CME initiation.

To simultaneously evolve a realistic model convection zone and corona at any spatial scale presents a number of daunting challenges. The upper convection zone and low solar atmosphere are highly stratified — average thermodynamic quantities change by many orders of magnitude as the domain transitions from a relatively cool, turbulent regime below the visible surface, to a hot, magnetically-dominated and shock-dominated regime high in the corona. The physics of the gas transitions from a high- β plasma where the magnetic field is advected by the gas (away from strong active region complexes) to a low- β regime where the gas is constrained to move along magnetic field lines. In addition, the radiation field transitions from being optically thick to optically thin. Temporal and spatial scales are highly disparate. Large concentrations of magnetic flux are compressed within intergranular lanes and evolve at convective turnover timescales, while large coronal loops form and persist for days as active regions emerge and evolve over a course of many months. In addition, the large-scale magnetic structure of the corona can change in a fraction of a second, as small-scale localized magnetic reconnection suddenly reorganizes the large-scale field, often triggering eruptive events along the way.

The corona presents particular challenges. It is well known that in order to accurately reflect the thermodynamics of this region, a model should include the effects of electron heat conduction along magnetic field lines and radiative cooling in the optically thin “coronal approximation”. In addition, some physics-based (*e.g.*, Joule heating) or empirically based source of coronal heating must be present (often introduced at the lower photospheric boundary) if the model corona is to remain hot. But to generate a realistic magnetic carpet, and to study the interaction of granular convection with coronal structures, requires there to be a turbulent model convection zone, and therefore some form of optically thick surface cooling.

In Abbett (2007) we introduced this physics into a 3D MHD convection-zone-to-corona model in the simplest, most computationally efficient way possible — we simply ignored the optically thick radiative transfer equation entirely, and instead used a parameterized Newton cooling function carefully calibrated against smaller-scale, more realistic radiative-MHD models of magneto-convection where the frequency-dependent LTE transfer equation was solved along with the MHD system (Bercik, 2002).

This approach has been successful in studying the structure of quiet-Sun magnetic fields and active region flux emergence (Abbett, 2007; Fang *et al.*, 2010a; Fang *et al.*, 2010b). Yet this treatment, while computationally efficient, has a number of limitations. Its principle drawback is that it is ultimately *ad hoc* and requires other, more realistic simulations as a basis for calibration in order to get meaningful results. The simplified cooling is imposed at a particular height or over a range of gas density, and is not generated in a physical way as a function of optical depth. To address these limitations, we build upon a technique introduced by Abbett and Fisher (2010), and in Section 3 derive a simple, flux-conservative approximation to optically thick cooling that is based on the gray radiative transfer equation in LTE. We then incorporate a form of this efficient, physics-based approximation into the RADMHD convection-zone-to-corona model of Abbett (2007), which we briefly describe in Section 2. In Section 4 we present new models of an open-field coronal hole region, and study the transport of magnetic energy from below the surface into the corona. Finally, in Section 5 we summarize our results.

2. Numerical Methodology

The parallel code RADMHD solves the following MHD conservation equations semi-implicitly on a three-dimensional Cartesian mesh:

$$\frac{\partial \rho}{\partial t} + \nabla \cdot (\rho \mathbf{u}) = 0, \quad (1)$$

$$\frac{\partial \rho \mathbf{u}}{\partial t} + \nabla \cdot \left[\rho \mathbf{u} \mathbf{u} + \left(p + \frac{B^2}{8\pi} \right) \mathbf{I} - \frac{\mathbf{B} \mathbf{B}}{4\pi} - \mathbf{\Pi} \right] = \rho \mathbf{g}, \quad (2)$$

$$\frac{\partial \mathbf{B}}{\partial t} + \nabla \cdot (\mathbf{u} \mathbf{B} - \mathbf{B} \mathbf{u}) = -\nabla \times (\eta \nabla \times \mathbf{B}), \quad (3)$$

$$\frac{\partial e}{\partial t} + \nabla \cdot (e \mathbf{u}) = -p \nabla \cdot \mathbf{u} + \frac{\eta}{4\pi} |\nabla \times \mathbf{B}|^2 + \Phi + Q, \quad (4)$$

The components of the state vector have the usual definitions: ρ , \mathbf{u} , e , p , \mathbf{B} , and \mathbf{g} denote the gas density, velocity, internal energy per unit volume, gas pressure, magnetic field, and gravitational acceleration respectively. Here, we assume Gaussian units. The viscous stress tensor is assumed to be of the form $\Pi_{ij} = 2\rho\nu[D_{ij} - 1/3(\nabla \cdot \mathbf{u})\delta_{ij}]$, where $D_{ij} = 1/2(\partial u_i/\partial x_j + \partial u_j/\partial x_i)$ and δ_{ij} denotes the Kronecker delta function. The function $\Phi = \sum_{i,j} \Pi_{ij} D_{ij}$ represents the rate of energy dissipation through viscous diffusion, and ν and η refer to the coefficients of kinematic viscosity and magnetic diffusivity, respectively. These coefficients are assumed constant, and are set to values that correspond to the grid-scale viscous and resistive dissipation. The source term Q includes important energy sources and sinks such as radiative cooling, the divergence of the electron heat flux (in the portion of the domain representing the model transition region and corona), and any desired empirically based coronal heating function.

A complete discussion of the components of this energy source term is provided by Abbett (2007). The system is closed with a non-ideal equation of state, using tabular data provided by the OPAL project (Rogers, 2000). In this article, the portion of the domain corresponding to the corona is heated by the empirically based coronal heating function described in Abbett (2007), and the effects of Joule dissipation within this region are ignored.

The semi-implicit numerical scheme is parallelized on a domain-decomposed mesh, and the core technique is based on operator splitting with a high-order Crank–Nicholson temporal discretization. We treat the electron thermal conduction, viscous and Joule dissipation, and radiative losses implicitly using a Jacobian-Free Newton-Krylov (JFNK) solver, and require that the remainder of the system be treated explicitly using the Central Weighted Essentially Non-Oscillatory (CWENO) method of (Kurganov and Levy, 2000; Balbás and Tadmor, 2006). In this way, we remain Courant limited by the magnetosonic wavespeed, and can follow the dynamics of the system in a reliable way (we may choose to relax this constraint when evolving active region magnetic fields over longer timescales). Any local divergence error introduced into the magnetic field as a result of the CWENO central scheme is dissipated by adding an additional artificial source term proportional to $\nabla(\nabla \cdot \mathbf{B})$ to the induction equation. A detailed description of the numerical methodology employed by RADMHD can be found in Section 2 of Abbett (2007).

A number of enhancements and improvements have been incorporated into the RADMHD source code since its initial release in 2007. Most improvements are in the form of improved performance and robustness, better MPI load balancing and scaling, and other enhancements in the code’s speed and efficiency. Among the enhancements are: *i*) a simplified and improved table inversion and interpolation algorithm that is necessary to incorporate the OPAL data into the code’s non-ideal equation of state and the CHIANTI data (Young *et al.*, 2003) into the code’s treatment of optically thin radiative cooling; *ii*) a new adaptive error algorithm in the GMRES (Generalized Minimum RESidual) substep of the JFNK solver that greatly improves convergence rates; *iii*) a more robust, global non-linear CWENO weighting scheme in the explicit substep of RADMHD; and *iv*) an option to evolve $\log \rho$ rather than ρ itself via the following rewrite of Equation (1):

$$\frac{\partial \ln \rho}{\partial t} + \nabla \cdot (\mathbf{u} \ln \rho) = (\ln \rho - 1) \nabla \cdot \mathbf{u}. \quad (5)$$

Since the model atmosphere is highly stratified, this is often useful as a means of making the code more robust, while at the same time retaining the desired shock-capture characteristics of the numerical scheme. More details on these and other algorithmic improvements will be provided in a technical document under preparation for inclusion with the next release of the code.

In essence, however, the core numerical methods of RADMHD remain the same as that presented in Abbett (2007). In this article, we focus on the portion of the energy source term Q of Equation (4) that contains the approximation for optically thick radiative cooling.

3. An Approximate Treatment of Optically Thick Cooling

Radiative cooling drives surface convection and is a crucial contributor to the energy balance in the region of the solar atmosphere bridging the convection zone and corona. Yet a full frequency-dependent solution to the LTE radiative transfer equation can be computationally expensive for large-scale convection-zone-to-corona calculations, particularly for active region or filament models where timescales are such that the radiative cooling must be updated at intervals close to the MHD CFL limit. Here, we build upon the approach introduced by Abbett and Fisher (2010), and derive an approximate, frequency-integrated expression for optically thick radiative cooling that is based on the gray transfer equation in LTE. We begin by considering the net cooling rate for a volume of plasma at a particular location in the solar atmosphere:

$$R = \int d\Omega \int d\nu (\eta_\nu - \kappa_\nu I_\nu). \quad (6)$$

Here, Ω represents solid angle, and ν the frequency. The subscript ν indicates that the emissivity, opacity, and specific intensity (η_ν , κ_ν , and I_ν respectively) depend on frequency. If we define the source function S_ν as the ratio of the emissivity to opacity, and rearrange the order of integration, we can recast the net cooling rate in the following form

$$R = \int d\nu \kappa_\nu \int d\Omega (S_\nu - I_\nu). \quad (7)$$

We define the mean intensity as $J_\nu \equiv (1/4\pi) \int d\Omega I_\nu$ and note that the source function is independent of direction. This allows Equation (7) to be expressed as

$$R = 4\pi \int d\nu \kappa_\nu (S_\nu - J_\nu). \quad (8)$$

If we now assume a locally plane-parallel geometry, the formal solution for the specific intensity can be written as (*e.g.*, Mihalas, 1978)

$$I_\nu(\tau_\nu, \mu) = \int_0^\infty d\tau' \frac{e^{-|\tau_\nu - \tau'|/|\mu|}}{|\mu|} S_\nu(\tau'), \quad (9)$$

where μ refers to the cosine angle and τ_ν to the frequency-dependent optical depth. We can now recast the expression for the mean intensity in terms of an integral over optical depth and cosine angle,

$$J_\nu(\tau_\nu) = \frac{1}{2} \int_0^\infty d\tau' S_\nu(\tau') \int_0^1 d|\mu| \frac{e^{-|\tau_\nu - \tau'|/|\mu|}}{|\mu|}, \quad (10)$$

This allows the integral over μ to be evaluated and expressed in terms of an exponential integral function,

$$J_\nu(\tau_\nu) = \frac{1}{2} \int_0^\infty d\tau' S_\nu(\tau') E_1(|\tau_\nu - \tau'|). \quad (11)$$

Up to now, no approximation other than an assumption of a locally plane parallel geometry has been made. We now follow the analysis of Abbett and Fisher (2010) and note that the first exponential integral function $[E_1(|\tau_\nu - \tau'|)]$ in Equation (11) is singular when $\tau' = \tau_\nu$, and that this singularity is integrable. Since E_1 is peaked around τ_ν , contributions from $S_\nu(\tau')$ will be centered around $S_\nu(\tau_\nu)$. Thus, to lowest order we can approximate the mean intensity by

$$J_\nu(\tau_\nu) \approx \frac{1}{2} S_\nu(\tau_\nu) \int_0^\infty d\tau' E_1(|\tau_\nu - \tau'|). \quad (12)$$

The integral over optical depth is now easily evaluated, and the result is expressed in terms of the second exponential integral function $[E_2]$:

$$J_\nu(\tau_\nu) \approx S_\nu(\tau_\nu) \left(1 - \frac{E_2(\tau_\nu)}{2} \right). \quad (13)$$

We now rearrange the terms in the above equation, and substitute $1 - J_\nu(\tau_\nu)/S_\nu(\tau_\nu) \approx E_2(\tau_\nu)/2$ into Equation (8), to arrive at an approximation for the net cooling rate,

$$R \approx 2\pi \int d\nu \kappa_\nu S_\nu E_2(\tau_\nu). \quad (14)$$

If we further assume LTE, the source function can be expressed as the Planck function $[B_\nu(T)]$ coupling the cooling rate to the local temperature of the plasma $[T]$:

$$R \approx 2\pi \int d\nu \kappa_\nu B_\nu(T) E_2(\tau_\nu). \quad (15)$$

We now integrate Equation (15) over frequency. Since $E_2(\tau_\nu)$ is bounded below by zero and above by unity, the integral in Equation (15) obeys this set of inequalities:

$$2\bar{\kappa}\sigma T^4 > 2\pi \int d\nu \kappa_\nu B_\nu(T) E_2(\tau_\nu) > 0, \quad (16)$$

where $\bar{\kappa}$ is the Planck-weighted mean opacity.

Because of the range of the $E_2(x)$ function, we can use this inequality to write the integral in Equation (15) in the form $R(\bar{\tau}) = 2\bar{\kappa}C(\bar{\tau})\sigma T^4 E_2(\alpha(\bar{\tau})\bar{\tau})$, where in general, α is a positive, unknown function of mean optical depth $\bar{\tau}$ ($d\bar{\tau} \equiv -\bar{\kappa}dz$), and $C(\bar{\tau})$ is an unknown, $\bar{\tau}$ -dependent normalization constant. However, since we expect a close relationship between the mean optical depth $\bar{\tau}$ and the local mean opacity $\bar{\kappa}$, we therefore make the ansatz that α is a constant, but with an unknown value. The expression for R can then be written

$$R \approx 2C\bar{\kappa}\sigma T^4 E_2(\alpha\bar{\tau}), \quad (17)$$

where C now represents a $\bar{\tau}$ -independent normalization constant of integration.

To determine the normalization constant C , we integrate our cooling function from zero to infinity in optical depth over an isothermal slab to obtain the total radiative flux. The resulting expression must be equal to the known result

$F_{\text{tot}} = \sigma T^4$, thus requiring $C = \alpha$. To calibrate α , we compare the cooling rate as a function of depth in test models using this approximation against more realistic models of magnetoconvection where the frequency-dependent transfer equation is solved in detail (Bercik, 2002). We conclude that the best-fit value is $\alpha = 1$ (see Figure 1 of Abbett and Fisher, 2010). This implies that optical depth in highly stratified atmospheres is dominated by the local opacity.

With the parameter α specified, we arrive at an approximation for optically thick surface cooling,

$$R \approx 2 \bar{\kappa} \sigma T^4 E_2(\bar{\tau}). \quad (18)$$

This expression can be efficiently evaluated at each iteration of an MHD calculation, and we have implemented this volumetric cooling rate as a part of the cell-centered source term Q in Equation (4) (the cooling rate R being a negative heating rate Q).

It is possible for the computational grid to be of sufficient resolution to resolve the local pressure scale heights of a highly stratified model atmosphere while at the same time being poorly resolved in optical depth. This has the potential to lead to numerical error in the calculation of the local cooling rate such that the total radiative flux may not be conserved. We therefore consider a flux conservative formulation similar to the constrained transport schemes common to many MHD codes (see Stone and Norman, 1992).

We begin by defining a frequency-independent discretized, optical depth for each iteration where the MHD state variables are updated. Since our simple approximation is based on the assumption of a locally plane-parallel geometry, and we are neglecting (for now) the effects of sideways transport, all that is required is an integration along the vertical direction (*i.e.*, in the direction of the gravitational acceleration). Our discretized expression takes the form

$$\tau_{i,j,k-1/2} \equiv \sum_{n=k_{top}}^k \bar{\kappa}_{i,j,k} (z_{n+1/2} - z_{n-1/2}) \quad (19)$$

Here, the grid coordinates i, j, k are defined at cell centers (consistent with the centralized numerical scheme implemented in RADMHD), and the optical depth is defined at face centers of the mesh cell's control volume perpendicular to the z -direction (we now drop the overbar notation, since the above definition makes it clear that τ is a frequency-averaged quantity). We use tabular Planck-weighted mean opacities ($\bar{\kappa}_{i,j,k}$) provided by the opacity project (Seaton, 2005). The coordinate k_{top} refers to the first ghost cell of the upper coronal boundary of the simulation domain, though in practice it is set to an interior cell bounding the portion of the domain that represents the optically thin corona. Either way, it is presumed that $\tau_{i,j,k_{top}-1/2} = 0$. Note that optical depth increases inward into the atmosphere in the opposite sense of the height z , which is defined to increase outward from the interior toward the visible surface (*i.e.*, $d\tau \equiv -\bar{\kappa} dz$).

The radiative cooling of Equation (18) can be expressed in terms of a divergence of a radiative flux. Our treatment of radiative transfer assumes a locally plane-parallel geometry, thus we need only consider the radiative flux at the

faces of control volumes normal to the vertical direction. This implies that any horizontal divergence of the radiative flux is assumed negligible when compared to gradients in the vertical direction. The physical justification for this simplification is that changes in emissivity and opacity are generally much greater in the vertical direction of a highly stratified atmosphere than those expected in the transverse direction. This assumption will likely not be valid at the edges of sunspots where the lateral emissivity and opacity gradients are expected to be large. Given this simplification, the divergence of the radiative flux can be expressed as

$$\frac{\partial F}{\partial z} = 2\bar{\kappa}\sigma T^4 E_2(\tau). \quad (20)$$

We now cast this expression in terms of optical depth $d\tau \equiv -\bar{\kappa}dz$:

$$\frac{\partial F}{\partial \tau} = -2\sigma T^4 E_2(\tau), \quad (21)$$

and note that this equation is of the form $Q(\tau) = -f(\tau)E_2(\tau)$ with $f(\tau) \equiv 2\sigma T^4$. We now approximate $f(\tau)$ with a Taylor-series expansion centered about τ_k accurate up to second order, and reorder the terms so that the expression is of the form $f(\tau) = A + B\tau$:

$$f(\tau) = [f(\tau_k) - \tau_k f'(\tau_k)] + \tau f'(\tau_k). \quad (22)$$

Here, $f(\tau_k) = 2\sigma T^4(\tau_k)$ refers to the function $f(\tau)$ evaluated at cell center coordinate (i, j, k) , $f'(\tau_k)$ refers to the function's vertical derivative with respect to optical depth evaluated at the same location, and the constants A and B have the form $A = [f(\tau_k) - \tau_k f'(\tau_k)]$ and $B = f'(\tau_k)$. For brevity, we have dropped the i and j subscripts, but note that these expressions are valid for all grid cells at a particular height.

To obtain the discretized form of Equation (21), we integrate over the control volume of the computational cell,

$$F(\tau_{k+1/2}) - F(\tau_{k-1/2}) = - \int_{\tau_{k-1/2}}^{\tau_{k+1/2}} (A + B\tau) E_2(\tau) d\tau. \quad (23)$$

This integral can be evaluated using the relation $dE_n(\tau)/d\tau = -E_{n-1}(\tau)$ to obtain

$$\begin{aligned} F(\tau_{k+1/2}) - F(\tau_{k-1/2}) &= A [E_3(\tau_{k+1/2}) - E_3(\tau_{k-1/2})] \\ &+ B [\tau_{k+1/2} E_3(\tau_{k+1/2}) - \tau_{k-1/2} E_3(\tau_{k-1/2}) \\ &+ E_4(\tau_{k+1/2}) - E_4(\tau_{k-1/2})]. \end{aligned} \quad (24)$$

All that remains is to define a stencil to evaluate $f(\tau_k)$ and $f'(\tau_k)$ in the expressions for A and B . RADMHD employs a central scheme, and it is desirable to derive a stencil consistent with the formalism of the code. Since the temperature T is obtained via a table lookup based on cell-centered values of gas density and internal energy per unit volume, we obtain our interpolation stencil by expanding

elements of the state vector $q(\tau)$ in a second-order accurate Taylor series about τ_k ,

$$q(\tau) = a + b(\tau - \tau_k) + \frac{c}{2}(\tau - \tau_k)^2, \quad (25)$$

and enforce the definition of cell-averaged quantities along the z -coordinate axis [again, the (i, j) dependence is implicitly assumed, and $\Delta\tau \equiv \tau_{k+1/2} - \tau_{k-1/2}$ is less than zero],

$$q_k = \frac{1}{\Delta\tau} \int_{\tau_{k-1/2}}^{\tau_{k+1/2}} q(\tau) d\tau. \quad (26)$$

We then expand about each of the points τ_{k+1} , τ_k , and τ_{k-1} ; substitute the appropriate form of Equation (25) into Equation (26); then perform the integration over each respective control volume. This yields a system of equations whose solution specifies a , b , and c in terms of known cell averages. The compact stencils are equivalent to those of Abbett (2007), and have the form $a = q_k - (q_{k+1} - 2q_k + q_{k-1})/24$, $b = (q_{k+1} - q_{k-1})/(2\Delta\tau)$, and $c/2 = (q_{k+1} - 2q_k + q_{k-1})/(\Delta\tau)^2$. The second term of a arises from the integration of the second-order term in the Taylor expansion of $q(\tau)$, and ensures that the interpolation scheme maintains second-order accuracy, and that the following discretized, cell-centered forms of A and B have desirable stability properties:

$$A = f_k - \frac{1}{24}(f_{k+1} - 2f_k + f_{k-1}) - \tau_k \frac{1}{2\Delta\tau}(f_{k+1} - f_{k-1}) \quad (27)$$

$$B = \frac{1}{2\Delta\tau}(f_{k+1} - f_{k-1}). \quad (28)$$

Here $f_k = 2\sigma T_k^4$, and $\tau_k = \tau_{k-1/2} - \kappa_k(\Delta z/2)$. With A and B specified, we arrive at an expression for a flux-conservative approximation to the optically thick radiative source term,

$$\begin{aligned} Q(\tau_{i,j,k}) &= A\bar{\kappa}_{i,j,k} [E_3(\tau_{i,j,k-1/2}) - E_3(\tau_{i,j,k+1/2})] \\ &\quad + B\bar{\kappa}_{i,j,k} [\tau_{i,j,k-1/2} E_3(\tau_{i,j,k-1/2}) - \tau_{i,j,k+1/2} E_3(\tau_{i,j,k+1/2}) \\ &\quad + E_4(\tau_{i,j,k-1/2}) - E_4(\tau_{i,j,k+1/2})]. \end{aligned} \quad (29)$$

By design, this expression will conserve flux to machine roundoff, as can easily be verified by showing that $Q_k + Q_{k-1} = F_{k+1/2} - F_{k-3/2}$ for all points (i, j, k) . Thus, we have two ways of implementing our approximation — the flux conservative approach of Equation (29), and the non-conservative approach obtained by directly evaluating Equation (18) using cell-centered quantities. The flux-conserving method requires additional table lookups each iteration to evaluate the exponential integrals, but is helpful in cases where the optical depth scale is not particularly well-resolved.

Our approximation for gray LTE cooling is applied only in those regions of the computational domain where such an approximation is needed. Specifically, we apply the approximation over a range of optical depths that extend from $\tau = 10$ to $\tau = 0.1$. At greater optical depths, we use the diffusion approximation (with

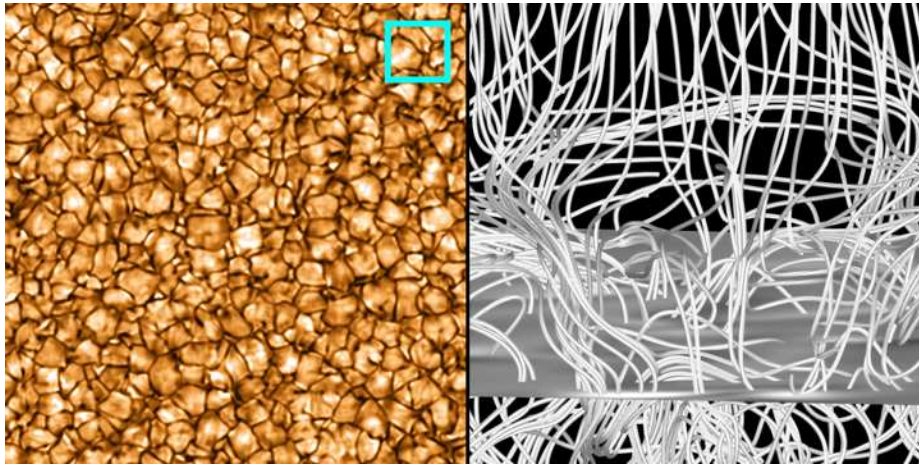


Figure 1. Left: Temperature at the RADMHD model photosphere. Right: Magnetic fieldlines threading the low atmosphere over a small sub-domain (the box in the left frame indicates the approximate size of the corresponding sub-domain). The gray slice indicates the average height of the visible surface. The domain spans $24 \times 24 \times 12 \text{ Mm}^3$ at a resolution of $512 \times 512 \times 256$.

tabular Rosseland mean opacities provided by Seaton, 2005), and at smaller optical depths we use the optically thin approximation (using CHIANTI data from Dere *et al.*, 1997 and Young *et al.*, 2003 to specify the optically thin cooling curve) as described in Abbett (2007) and Lundquist, Fisher, and McTiernan (2008).

The simulations we present in Section 4 use the non-conservative technique. The conservative approach described above was motivated by the fact that in some cases, where the model atmosphere is poorly resolved in optical depth, the strong cooling prescribed by Equation (18) can be concentrated in a narrow one- or two- zone layer of a model atmosphere. As a practical matter, this required that we enforce a limit on the maximum amount of cooling per unit mass allowable in any given grid cell. This cooling floor is somewhat artificial, and is not necessary in the flux conservative method, which has the effect of spreading the cooling over adjoining cells in a more physical way. Another option would be to have a separate grid for optical depth, but we decided against this because of the possibility of introducing additional interpolation error that is difficult to characterize. We are currently testing our new flux-conservative scheme, and plan to fully implement it in a new radiation subroutine for RADMHD that also includes the important effects of sideways transport. We hope to report on these efforts in the near future.

4. A Model of an Open Flux Region

We initiate our calculations using the procedure of Abbett (2007). Briefly, we begin by relaxing a 1D-symmetric average stratification, then expand the domain to three dimensions and break the 1D symmetry by introducing a small, random

energy perturbation in the superadiabatically stratified portion of the computational domain representing the solar convection zone. Convective turbulence develops as the simulations progress, and we allow the model convection zone to dynamically relax. We show results from two separate simulations: one was performed locally using 112 processors of a relatively small Beowulf cluster, and the other was performed on NASA's Discover supercomputer using 512 processors. Both simulations simultaneously evolve a model convection zone and corona, and each domain has a vertical extent of 12 Mm, with a 2.5 Mm deep model convection zone. The development model that was run on the local Beowulf cluster has a domain that spans $21 \times 12 \times 12 \text{ Mm}^3$ at a resolution of $448 \times 256 \times 256$, while the larger run on Discover spans $24 \times 24 \times 12 \text{ Mm}^3$ at a relatively high resolution of $512 \times 512 \times 256$. In each case, only ≈ 0.66 percent of the total computational effort was expended by the approximate treatment of the radiative transfer on average within any given MPI subdomain during a given timestep. On the Intel Xeon E5420 CPUs of our local Beowulf cluster, the computing time per update of this substep is approximately 0.03 core-microseconds per point. The simulations presented here should be considered relatively small-scale in the context of the capability of the algorithms presented — the code scales well on multiple processors, and once our development work is complete we intend to dramatically extend the spatial scale of the models.

The simulations presented here differ from those of Abbett (2007) in a fundamental way. The approximation we now use for optically thick cooling eliminates all of the *ad-hoc* calibrated parameters present in the older models. Specifically, the height and magnitude of the optically thick radiative source term is now calculated in a physically self-consistent way based on an optical-depth scale rather than on an specified density or height range attenuated by envelope functions (*c.f.* Section 2.1.1 of Abbett, 2007). Once α of Equation (17) has been calibrated against more realistic models, no further adjustment is required, and each atmosphere relaxes to a state determined by the solution of the system of Equations (1)-(4) subject to imposed boundary conditions.

We apply periodic boundaries in the horizontal directions, and a simple, somewhat-artificial closed lower boundary. Specifically, the internal energy per unit volume within ghost cells adjacent to the domain's lower boundary is set such that a temperature gradient is maintained that best matches the average stratification at a corresponding height in the Bercik (2002) magnetoconvection models. In addition, the ghost cells at the lower boundary are specified such that the vertical components of the velocity and magnetic field and the vertical gradients of the horizontal components of the velocity and magnetic field are zero, and such that the gradient of the gas density is maintained. The upper coronal boundary is initially taken to be anti-symmetric during the relaxation procedure (*i.e.*, ghost zones are set such that the vertical component of the velocity and magnetic field vanishes at the boundary while all other components of the MHD state vector maintain a zero vertical gradient across the boundary interface), then is set to a standard zero-gradient boundary condition once magnetic fields are introduced (*i.e.*, ghost cells are set such that all components of the MHD state vector maintain a zero vertical gradient across the upper boundary interface). For the simulations presented here, once the purely hydrodynamic

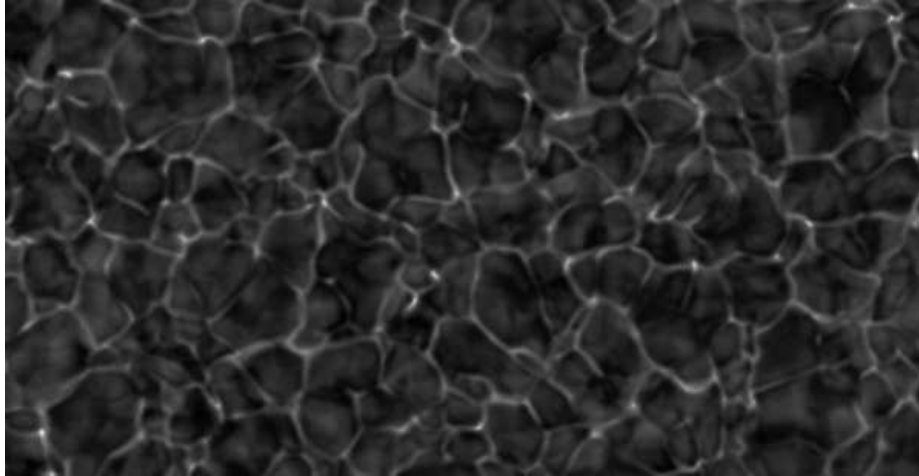


Figure 2. Temperature in the RADMHD low chromosphere showing a reverse granulation pattern. Lighter (darker) colors indicate hotter (cooler) temperatures. In the models, this occurs because the radiative cooling diminishes with height, and the $\mathbf{p}\nabla \cdot \mathbf{v}$ work of converging and diverging flows above the intergranular lanes begins to dominate. The horizontal slice spans $21 \times 12 \text{ Mm}^2$ at a resolution of 448×256

model convection zone is relaxed, we introduce a weak 1 G vertically directed magnetic field. This is intended to create an open-flux region, such as one might expect within a coronal hole.

As the simulations progress, the convective turbulence acts to stretch and amplify the field, and the portion of the domain representing the corona begins to heat as a result of the magnetic-field-dependent empirically-based coronal-heating source term. This heating function is based on the Pevtsov *et al.* (2003) power-law relationship between X-ray luminosity and total unsigned magnetic flux observed at the surface (see Equation 12 of Abbett, 2007). For this study, we are content to rely on empirical heating rather than Joule dissipation to energize the model corona since our focus is on the transport of magnetic energy into the atmosphere, not the heating of the low atmosphere and corona.

Up to the point that magnetic field was introduced into the simulation domain, the model corona was simply an unphysical, cold, nearly evacuated region. Once the corona heats, we activate the implicit electron thermal conduction source term. This builds a corona, but reduces our timestep somewhat since the stiffness of the system is increased and convergence rates in the JFNK substep can become an issue. Thus, it tends to be the last step of our relaxation process. After several additional turnover times, we begin our analyses.

The left frame of Figure 1 shows the temperature at the visible surface ($\tau = 1$) of a relaxed convection zone-to-corona model using the new formalism of Section 3. The granular pattern and convective turnover times compare well to the realistic magnetoconvection models of Bercik (2002). This, along with the reverse granulation pattern shown in Figure 2, indicates that our approximation

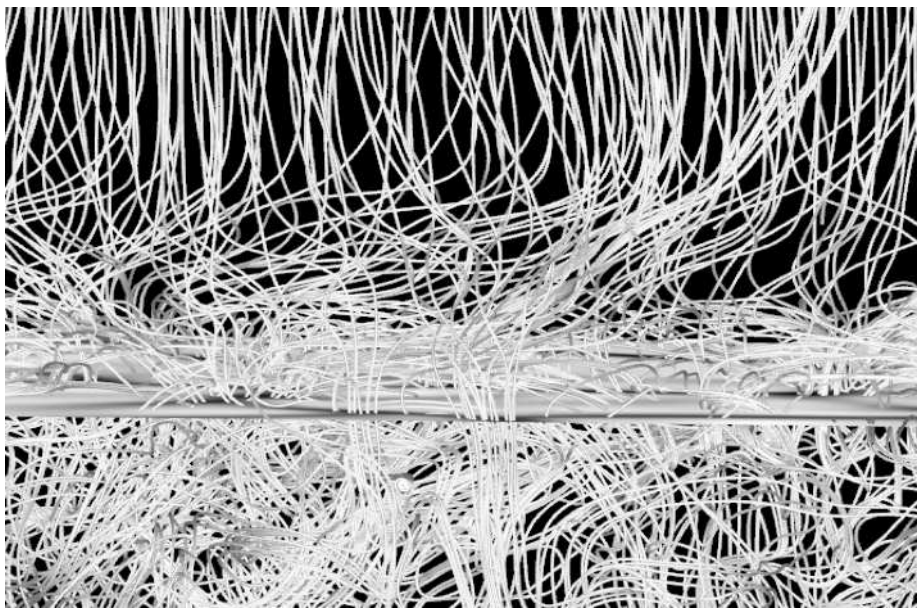


Figure 3. Magnetic fieldlines threading the low atmosphere over a portion of the computational domain. The gray slice represents the approximate position of the model's visible surface. Horizontally directed magnetic fields due to the spreading of canopy-like structures and overturning convective cells permeate the low atmosphere.

to optically thick radiative transfer is capturing the physics of surface cooling at least well enough to generate and sustain solar-like convective features.

The right frame of Figure 1 shows the complex magnetic structure threading a small portion of the simulation domain (as indicated by the cyan box in the upper-right corner of the left frame). Figure 3 shows a larger subdomain at a later time, and more clearly illustrates the characteristics of the magnetic structure. In the region where convective cells turn over, the average plasma- β remains relatively high. As a result, much of the magnetic field remains entrained in the plasma, turns over, and is recirculated back below the surface. Thus, at any given time, this region is filled with horizontally directed field, and that field tends to be less concentrated than is typical of fields entrained in the vortical downdrafts present at the visible surface and below. In addition, the presence of canopy-like structures (where strong concentrations of field above intergranular lanes and photospheric downdrafts open into the upper atmosphere and spread out like a fan) also contribute to the net amount of horizontally directed magnetic field threading the atmosphere below the corona.

The presence of horizontal fields in the atmosphere has consequences for the transport of magnetic energy into the upper atmosphere. Consider the electromagnetic Poynting flux,

$$\mathbf{S} = \frac{1}{4\pi} c \mathbf{E} \times \mathbf{B}. \quad (30)$$

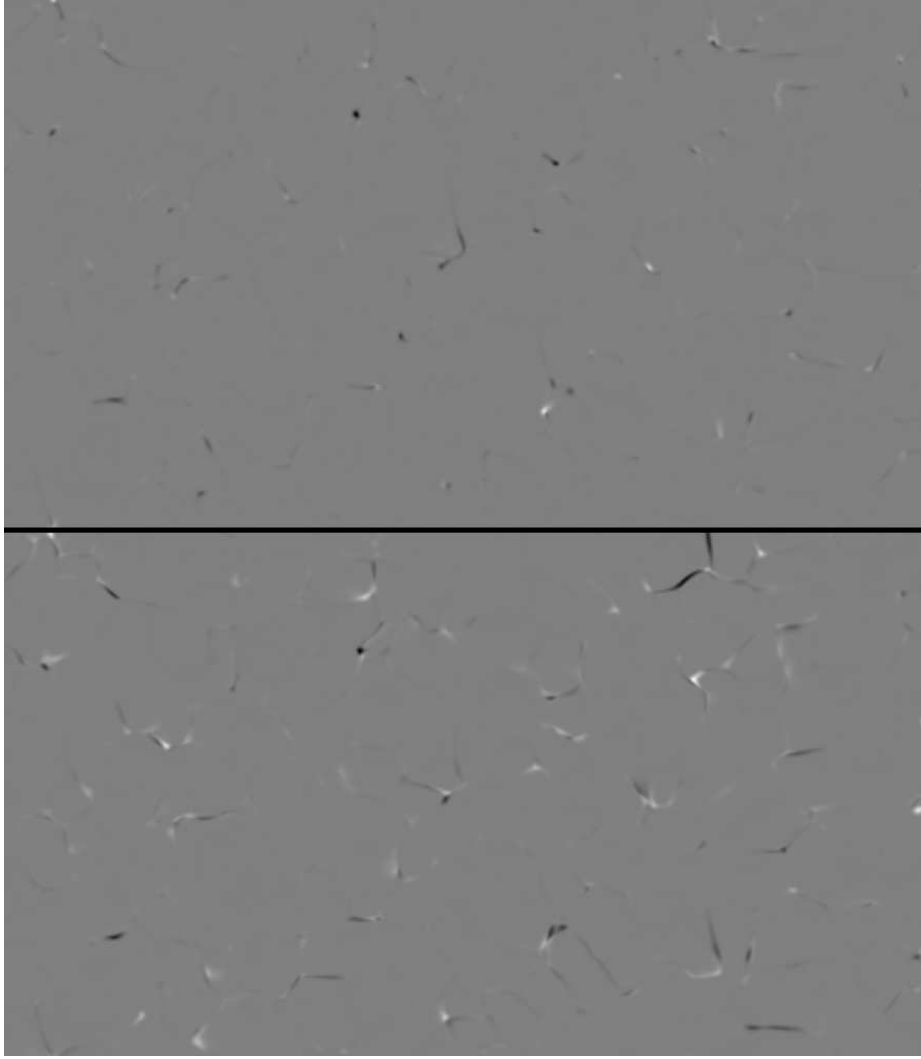


Figure 4. The vertical component of the Poynting flux along a layer positioned just below optical depth unity (top) and 400 km higher near the tops of overturning granules (bottom). Light colors correspond to outward directed flux (toward the corona); dark colors represent inward-directed flux (toward the convective interior). Each slice spans $21 \times 12 \text{ Mm}^2$.

The vertical component of the Poynting flux is a measure of the amount of electromagnetic energy flowing into, or out of the solar atmosphere from below the surface where it is generated. In Figure 4, we display S_z as a grayscale image at two layers in the model atmosphere — dark shades correspond to a flux of magnetic energy directed toward the interior, while lighter shades correspond to an outward-directed flux. The top frame shows the vertical component of Poynting flux along an x - y slice positioned just below the visible surface, and the lower frame shows S_z along a slice positioned in the low atmosphere, 400 km

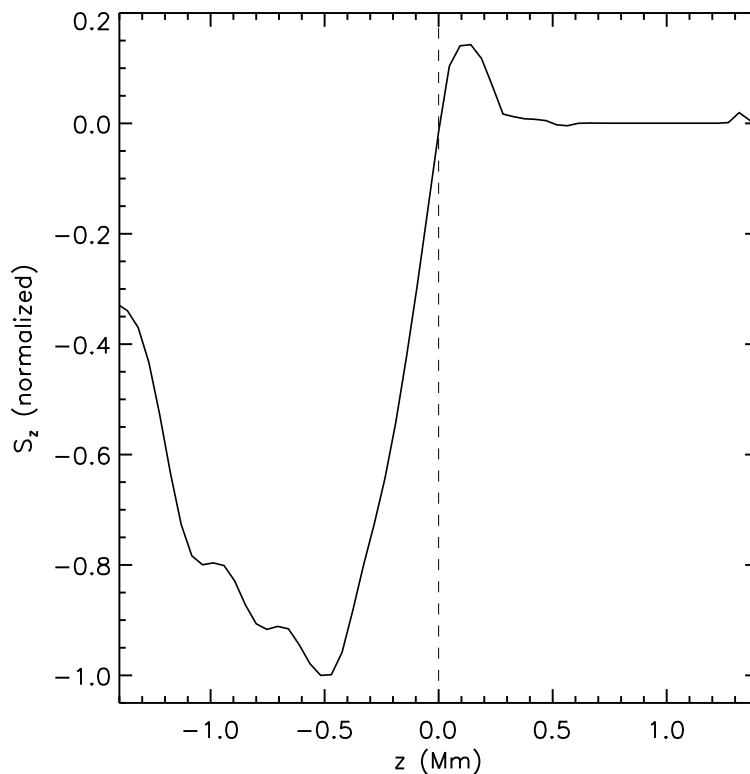


Figure 5. The normalized net vertical component of the Poynting flux over a portion of the domain centered at the model’s photosphere. The dashed vertical line represents the approximate height of the visible surface. Above the visible surface, electromagnetic energy tends to flow outward toward the corona, while below the surface, energy flows inward toward the convective interior. Above $z \approx 0.5$ (in the model’s low chromosphere) the Poynting flux tends to remain outwardly directed, but its magnitude is, on average, less than a percent of its maximum value.

higher. Careful examination of Figure 4 reveals an imbalance in the outward- and inward-directed flux. Below the surface, there appears to be a net flow of magnetic energy into the convective interior along the strong vortical downdrafts contained within intergranular lanes. Conversely, in the low atmosphere, the vertical component of the Poynting flux appears more diffuse, and there appears to be a net excess of outward directed flux, particularly within overturning granules.

This is shown more clearly in Figure 5 where S_z is integrated over each layer in the computational domain, and plotted as a normalized quantity as a function of height $[z]$. The dashed vertical line in the figure represents the average height of the visible surface. What is clear, is that magnetic energy on average is directed downward into the interior below the visible surface. It is at the surface and above that the net vertical Poynting flux changes sign and becomes outwardly directed. This suggests that the kinetic motion of overturning granules in the

model's overshoot layer provides the source of magnetic energy for the corona, not the deeper layers below the optical surface, where magnetic flux and energy are being pumped down into the interior along intergranular downflows.

This can be understood in a fairly straightforward way. The vertical component of the Poynting flux can be expressed as

$$S_z = \frac{1}{4\pi} (c\mathbf{E}_h \times \mathbf{B}_h) \cdot \hat{\mathbf{z}}, \quad (31)$$

where \mathbf{E}_h and \mathbf{B}_h refer to the horizontal components of the electric and magnetic field respectively. If we assume ideal MHD, then the horizontal component of the electric field can be written as follows:

$$c\mathbf{E}_h = -u_z \hat{\mathbf{z}} \times \mathbf{B}_h - \mathbf{u}_h \times B_z \hat{\mathbf{z}}. \quad (32)$$

Just above the visible surface, the magnetic field remains entrained in the fluid as convective cells overturn. At this height, the strongest field concentrations are located near the edges of overturning granules as divergent flows from neighboring cells compress the field. On average, there is more of a contribution to the horizontal electric field from the second term of Equation (32), $c\mathbf{E}_h = -\mathbf{u}_h \times B_z \hat{\mathbf{z}}$, since the magnetic field becomes more vertical as converging flows compress flux into a relatively small area. The contribution of this term to the vertical component of the Poynting flux can be expressed as $4\pi S_z = [(-\mathbf{u}_h \times B_z \hat{\mathbf{z}}) \times \mathbf{B}_h] \cdot \hat{\mathbf{z}}$. Simplified, this becomes $4\pi S_z = -B_z (\mathbf{B}_h \cdot \mathbf{u}_h)$.

To illustrate the correlation between the horizontal magnetic fields $[\mathbf{B}_h]$ and the converging surface flows $[\mathbf{u}_h]$, consider a weak, vertically oriented, untwisted magnetic flux tube that passes through the surface. Suppose it is acted on by a strong converging flow in a thin layer at the surface. If the magnetic field of the tube is oriented in the positive z direction, then just above the surface, the compression will tilt the fieldlines and create horizontal components of the magnetic field in the opposite direction of the converging flow. If the magnetic field is oriented in the negative z direction, then the horizontal components of the field will be aligned with the flow. Either way, $4\pi S_z = -B_z (\mathbf{B}_h \cdot \mathbf{u}_h)$ is positive above the surface. Obviously, the dynamics of the model are far more complex than this simple thought experiment. Nevertheless, we do find a net positive contribution to the Poynting flux from the second term of Equation (32) along the edges of overturning granules above the surface where the field is being compressed.

Below the photosphere, the situation is quite different. The strongest magnetic fields are concentrated within localized vortical downdrafts. The asymmetry between these strong downdrafts and the broad upwelling plasma in stratified convection is well known, and may provide a mechanism whereby magnetic flux can be pumped into the interior (Tobias *et al.*, 2001). We find more of a contribution to the net Poynting flux from the first term of Equation (32), $4\pi S_z = [(-u_z \hat{\mathbf{z}} \times \mathbf{B}_h) \times \mathbf{B}_h] \cdot \hat{\mathbf{z}}$. This can be expressed more simply as $4\pi S_z = u_z B_h^2$, and in this form, it is easy to see that a net downward transport of magnetic flux is consistent with a net downward-directed Poynting flux. This downward-directed flux of electromagnetic energy below the surface is consistent with other simulations of radiative-magnetoconvection (see, *e.g.*, Vögler and Schüssler, 2007).

The first to recognize this change in direction of the flow of electromagnetic energy was Steiner *et al.* (2008) who referred to the visible surface as “a separatrix for the vertically directed Poynting Flux”. Our results are consistent with their findings, although we conclude that in the larger domain, the upward-directed net flow of magnetic energy tends to arise from the action of the compressive flows of overturning convection as magnetic flux is expelled from cell centers and concentrated into the intergranular regions. However, higher in the model atmosphere as the gas transitions to a low- β regime (the upper chromosphere–transition region boundary), we also see a small buildup of magnetic flux, for reasons similar to those of Steiner *et al.* (2008). Namely, that the dynamic chromosphere transitions to a stable, subadiabatic, magnetically-dominated regime, and there is a magnetic reservoir on average as magnetic flux that is advected upward enters the stable regime and does not get recirculated back into the convective interior (similar in some ways to the overshoot layer at the base of the convection zone). This is reflected in the small peak in Figure 5 at a height of ≈ 1.3 Mm above the visible surface. Above this transition region interface in the open field of the model corona, energy is transported via magnetosonic and Alfvén waves. We note that in these simulations, the magnetic field has yet to fully saturate (*i.e.*, there is a small increase in magnetic energy over time as magnetic field is stretched and amplified by convective turbulence). While this indicates that the atmosphere has yet to fully relax, this increase in magnetic energy (and any Joule heating below the corona) is negligible in comparison to the divergence of the Poynting flux and the work done on the magnetic field by convective motions.

In some sense, the height at which the transition between outward and inward flow of electromagnetic energy takes place is less important than the fact that such a transition exists. What the simulations seem to suggest is that in quiescent regions away from particularly strong concentrations of magnetic flux, there is not a continuous flow of electromagnetic energy from below the surface out into the corona. Instead, the mechanical energy of convection mediates the flow of magnetic energy in the relatively high- β surface layers where the magnetic field remains frozen into the plasma. Of course, in and around very strong concentrations of magnetic flux, the situation is undoubtedly quite different.

5. Discussion and Conclusions

We have developed an approximate treatment of optically thick radiative surface cooling that successfully reproduces the average thermodynamic stratification of smaller scale, more realistic numerical models where the frequency-dependent radiative transfer equation in LTE is solved in detail. This technique retains the computational efficiency of earlier parameterized methods, but does not require continual calibration against more realistic simulations. We find that with the new method we are able to initiate and sustain a stable convection pattern with a distribution of cell sizes and turnover times characteristic of solar granulation.

The method presents a middle ground between realistic radiative MHD models that solve the transfer equation in detail, and idealized models that simply

impose a thermodynamic stratification, or ignore the physics of radiative transport entirely. The motivation for developing this technique is to make feasible physics-based large-scale or global parameter space studies of the interaction of active region-scale magnetic fields with the small scale fields associated with granular convection in a domain that includes both a convection zone and corona.

Whether the approximate treatment captures enough of the essential physics of the system still remains to be seen. The technique is certainly limited by the fact that sideways transport is ignored, and important physics of the chromosphere has yet to be included in the current models. Even so, we are able to generate solar-like convective turbulence in a physically self-consistent way, and follow the magnetic evolution of structures that thread the interface between the convective interior and corona.

In particular, we presented two simulations that confirm the existence of a “separatrix” in the flow of magnetic energy from the interior to the atmosphere (see Steiner *et al.*, 2008), and demonstrate that it is the mechanical energy of surface convection driven by strong radiative cooling that is the source of energy for this divergent flux of electromagnetic energy. In a quiescent region, in the absence of strong concentrations of magnetic flux, our models suggest that it is the low photosphere that provides the source of electromagnetic energy to the chromosphere and corona, not the sub-surface layers.

Acknowledgments: This research was funded in part by the NASA Heliophysics Theory Program (grant NNX08AI56G), the NASA Living-With-a-Star TR&T Program (grant NNX08AQ30G), and the NSF’s AGS Program (grant ATM-0737836). The authors wish to acknowledge Dick Canfield’s pioneering efforts in the development of radiation hydrodynamics during the 1970s and 1980s. The particular description in this paper for the simplified radiative cooling treatment was inspired by the very first work (unpublished) that GHF did for Dick Canfield as a graduate student, namely an investigation of escape probability treatments for continuum radiation processes. Indeed, it is possible to derive the radiative cooling treatment described here using escape probability concepts.

References

- Abbett, W.P.: 2007, The Magnetic Connection between the Convection Zone and Corona in the Quiet Sun. *Astrophys. J.* **665**, 1469–1488. doi:10.1086/519788.
- Abbett, W.P., Fisher, G.H.: 2010, Improving large-scale convection-zone-to-corona models. *Mem. Soc. Astron. Ital.* **81**, 721–728.
- Abbett, W.P., Hawley, S.L.: 1999, Dynamic Models of Optical Emission in Impulsive Solar Flares. *Astrophys. J.* **521**, 906–919. doi:10.1086/307576.
- Allred, J.C., Hawley, S.L., Abbett, W.P., Carlsson, M.: 2005, Radiative Hydrodynamic Models of the Optical and Ultraviolet Emission from Solar Flares. *Astrophys. J.* **630**, 573–586. doi:10.1086/431751.
- Archontis, V., Hood, A.W.: 2010, Flux emergence and coronal eruption. *Astron. Astrophys.* **514**, 56–59. doi:10.1051/0004-6361/200913502.
- Balbás, J., Tadmor, E.: 2006, Nonoscillatory central schemes for one- and two-dimensional magnetohydrodynamics equations. ii: High-order semidiscrete schemes. *SIAM J. Sci. Comput.* **28**(2), 533–560. doi:10.1137/040610246. <http://link.aip.org/link/?SCE/28/533/1>.

- Bercik, D.J.: 2002, A numerical investigation of the interaction between convection and magnetic field in a solar surface layer. PhD thesis, Michigan State University.
- Carlsson, M., Stein, R.F.: 1992, Non-LTE radiating acoustic shocks and Ca II K2V bright points. *Astrophys. J. Lett.* **397**, 59–63. doi:10.1086/186544.
- Carlsson, M., Hansteen, V.H., Gudiksen, B.V.: 2010, Chromospheric heating and structure as determined from high resolution 3D simulations. *Mem. Soc. Astron. Ital.* **81**, 582–587.
- Cheung, M.C.M., Rempel, M., Title, A.M., Schüssler, M.: 2010, Simulation of the Formation of a Solar Active Region. *Astrophys. J.* **720**, 233–244. doi:10.1088/0004-637X/720/1/233.
- Dere, K.P., Landi, E., Mason, H.E., Monsignori Fossi, B.C., Young, P.R.: 1997, CHIANTI - an atomic database for emission lines. *Astron. Astrophys. Suppl.* **125**, 149–173.
- Fan, Y.: 2009, The Emergence of a Twisted Flux Tube into the Solar Atmosphere: Sunspot Rotations and the Formation of a Coronal Flux Rope. *Astrophys. J.* **697**, 1529–1542. doi:10.1088/0004-637X/697/2/1529.
- Fang, F., Manchester, W., Abbett, W.P., van der Holst, B.: 2010a, Simulation of Flux Emergence from the Convection Zone to the Corona. *Astrophys. J.* **714**, 1649–1657. doi:10.1088/0004-637X/714/2/1649.
- Fang, F., Manchester, W.B., Abbett, W.P., van der Holst, B., Schrijver, C.J.: 2010b, Simulation of Flux Emergence in Solar Active Regions. *AGU Fall Meeting Abstracts*, A1781.
- Fisher, G.H., Canfield, R.C., McClymont, A.N.: 1985, Flare loop radiative hydrodynamics. V - Response to thick-target heating. VI - Chromospheric evaporation due to heating by nonthermal electrons. VII - Dynamics of the thick-target heated chromosphere. *Astrophys. J.* **289**, 414–441. doi:10.1086/162901.
- Galsgaard, K., Archontis, V., Moreno-Insertis, F., Hood, A.W.: 2007, The Effect of the Relative Orientation between the Coronal Field and New Emerging Flux. I. Global Properties. *Astrophys. J.* **666**, 516–531. doi:10.1086/519756.
- Georgobiani, D., Zhao, J., Kosovichev, A.G., Benson, D., Stein, R.F., Nordlund, Å.: 2007, Local Helioseismology and Correlation Tracking Analysis of Surface Structures in Realistic Simulations of Solar Convection. *Astrophys. J.* **657**, 1157–1161. doi:10.1086/511148.
- Krasnoselskikh, V., Vekstein, G., Hudson, H.S., Bale, S.D., Abbett, W.P.: 2010, Generation of Electric Currents in the Chromosphere via Neutral-Ion Drag. *Astrophys. J.* **724**, 1542–1550. doi:10.1088/0004-637X/724/2/1542.
- Kurganov, A., Levy, D.: 2000, A third-order semidiscrete central scheme for conservation laws and convection-diffusion equations. *SIAM J. Sci. Comput.* **22**(4), 1461–1488.
- Lundquist, L.L., Fisher, G.H., McTiernan, J.M.: 2008, Forward Modeling of Active Region Coronal Emissions. I. Methods and Testing. *Astrophys. J. Supp.* **179**, 509–533. doi:10.1086/592775.
- Magara, T.: 2006, Dynamic and Topological Features of Photospheric and Coronal Activities Produced by Flux Emergence in the Sun. *Astrophys. J.* **653**, 1499–1509. doi:10.1086/508926.
- Manchester, W. IV, Gombosi, T., DeZeeuw, D., Fan, Y.: 2004, Eruption of a Buoyantly Emerging Magnetic Flux Rope. *Astrophys. J.* **610**, 588–596. doi:10.1086/421516.
- Martínez-Sykora, J., Hansteen, V., Carlsson, M.: 2008, Twisted Flux Tube Emergence From the Convection Zone to the Corona. *Astrophys. J.* **679**, 871–888. doi:10.1086/587028.
- Martínez-Sykora, J., Hansteen, V., Carlsson, M.: 2009, Twisted Flux Tube Emergence from the Convection Zone to the Corona. II. Later States. *Astrophys. J.* **702**, 129–140. doi:10.1088/0004-637X/702/1/129.
- McClymont, A.N., Canfield, R.C.: 1983, Flare loop radiative hydrodynamics. I - Basic methods. *Astrophys. J.* **265**, 483–506. doi:10.1086/160692.
- Mihalas, D.: 1978, *Stellar atmospheres 2nd edition*, San Francisco, W. H. Freeman and Co.
- Murray, M.J., Hood, A.W., Moreno-Insertis, F., Galsgaard, K., Archontis, V.: 2006, 3D simulations identifying the effects of varying the twist and field strength of an emerging flux tube. *Astron. Astrophys.* **460**, 909–923. doi:10.1051/0004-6361:20065950.
- Pevtsov, A.A., Fisher, G.H., Acton, L.W., Longcope, D.W., Johns-Krull, C.M., Kankelborg, C.C., Metcalf, T.R.: 2003, The Relationship Between X-Ray Radiance and Magnetic Flux. *Astrophys. J.* **598**, 1387–1391. doi:10.1086/378944.
- Rempel, M., Schüssler, M., Knölker, M.: 2009, Radiative Magnetohydrodynamic Simulation of Sunspot Structure. *Astrophys. J.* **691**, 640–649. doi:10.1088/0004-637X/691/1/640.
- Rogers, F.J.: 2000, Ionization equilibrium and equation of state in strongly coupled plasmas. *Phys. Plasmas* **7**, 51–58. doi:10.1063/1.873815.
- Seaton, M.J.: 2005, Opacity Project data on CD for mean opacities and radiative accelerations. *Mon. Not. Roy. Astron. Soc.* **362**, 1–3. doi:10.1111/j.1365-2966.2005.00019.x.

- Stein, R.F., Nordlund, Å.: 2006, Solar Small-Scale Magnetoconvection. *Astrophys. J.* **642**, 1246–1255. doi:10.1086/501445.
- Steiner, O., Rezaei, R., Schaffenberger, W., Wedemeyer-Böhm, S.: 2008, The Horizontal Internetwork Magnetic Field: Numerical Simulations in Comparison to Observations with Hinode. *Astrophys. J. Lett.* **680**, 85–88. doi:10.1086/589740.
- Stone, J.M., Norman, M.L.: 1992, ZEUS-2D: A Radiation Magnetohydrodynamics Code for Astrophysical Flows in Two Space Dimensions. II. The Magnetohydrodynamic Algorithms and Tests. *Astrophys. J. Supp.* **80**, 791–818. doi:10.1086/191681.
- Tobias, S.M., Brummell, N.H., Clune, T.L., Toomre, J.: 2001, Transport and Storage of Magnetic Field by Overshooting Turbulent Compressible Convection. *Astrophys. J.* **549**, 1183–1203. doi:10.1086/319448.
- Vögler, A., Schüssler, M.: 2007, A solar surface dynamo. *Astron. Astrophys.* **465**, 43–46. doi:10.1051/0004-6361:20077253.
- Young, P.R., Del Zanna, G., Landi, E., Dere, K.P., Mason, H.E., Landini, M.: 2003, CHIANTI—An Atomic Database for Emission Lines. VI. Proton Rates and Other Improvements. *Astrophys. J. Supp.* **144**, 135–152. doi:10.1086/344365.

